ITC 2/53
Information Technology and Control
Vol. 53 / No. 2 / 2024
pp. 522-541
DOI 10.5755/j01.itc.53.2.35152

Automated Retinal Image Analysis to Detect Optic Nerve Hypoplasia

Received 2023/09/20 | Accepted after revision 2024/02/13

HOW TO CITE: Celik, C., Yücedağ, İ., Akçam, H. T. (2024). Automated Retinal Image Analysis to Detect Optic Nerve Hypoplasia. *Information Technology and Control*, 53(2), 522-541. https://doi.org/10.5755/j01.itc.53.2.35152

Automated Retinal Image Analysis to Detect Optic Nerve Hypoplasia

Canan Celik
Faculty of Informatics, Duzce University, Department of Electrical-Electronics and Computer Engineering, Duzce, Turkey; phone: +90 0 380 731 20 45; fax: 0 380 731 31 24; e-mail: canancelik@duzce.edu.tr

İbrahim Yücedağ
Faculty of Informatics; D Duzce University, Department of Computer Engineering, Duzce, Turkey phone: +90 0 380 542 11 00; fax: 0380 542 11 03; e-mail: ibrahimyucedag@duzce.edu.tr

Hanife Tuba Akçam
Faculty of Informatics; Department of Ophthalmology, Ankara Yıldırım Beyazıt University, Ankara, Turkey; phone: +90 312 906 1000; fax: +90 312 906 2950; e-mail: htakcam@aybu.edu.tr

Corresponding author: canancelik@duzce.edu.tr

Identification of the optic disc and fovea is crucial for automating the diagnosis and screening of retinal diseases. Based on quantitative calculations, this study presents a decision support system for doctors that automatically detect optic nerve hypoplasia. For disease diagnosis, U-Net architecture is used, which uses a pre-trained ResNet encoder to segment the optic disc and fovea structures. An important aspect of the proposed technique is that pretrained ResNet and U-Net are used together, providing robust performance in the detection of optic nerve hypoplasia. Our proposed architecture was tested on retinal images from Messidor, Diaretdb1, DRIVE, HRF, APTOS, and IDRID. In addition, a special database called ONH-NET was created based on 189 retinal images obtained from Düzce University, Department of Ophthalmology. Messidor database test images showed, 0. 9069 IOU Score, 0.9626 Sensitivity, 0.9411 Precision, 0.9974 Accuracy and 0.9505 dice-coefficient values in optic disc detection, and 0.8282 IOU score, 0.8442 sensitivity, 0.8252 precision, 0.8992 Accuracy, 0.7873 dice coefficient values were obtained in fovea detection. We computed diameter optic disc to macula radius ratios from segmented optic disc and fovea for screening optic nerve hypoplasia and achieved 100% success.

KEYWORDS: Deep Learning, Image Segmentation, Optic Disc, Fovea, Macula, U-Net.

1. Introduction

An important layer of the eye is the retina, which can show signs of disease early. The majority of visual disorders are caused by structural deterioration of various structures in the retina layer of the eye (vessels, optic disc, macula, fovea, etc.) [2]. Fundus cameras with different settings are used to take retinal images.

There are three different modes for fundus cameras, including Color Fundus Retinal Imaging, Red-Free Imaging, and Fluorescent Angiography Imaging [4]. A fundus image provides insight into the anatomy of the eye's crucial structures, including the optic disc, blood vessels, macula and fovea. An essential anatomical structure in retinal fundus images is the optic disc (OD). According to fundus images, the OD appears bright, yellowish, and almost circular. It is where the main blood vessels enter the retina. It is difficult to get an accurate location or outline of OD with segmentation techniques because of the distractions in the images, such as abnormal lesions, imprecise boundaries, and peripapillary atrophy, despite OD being an approximate circle and having high intensity characteristics [11].

In Figure 1, OD appears as a bright disc-shaped area at the point where blood vessels gather 3-4 mm from the fovea, the macula's center. An area between superior and inferior temporal retinal arteries and veins that run tangential to OD is known as the macula. Figure 1 shows the macula's four topographic components: perifovea, parafovea, fovea, and foveolar [36]. The retina provides detailed central vision thanks to this small, highly sensitive area [35]. Located in the macula's center, the fovea is the most sensitive region of vision. This is part of the eye that controls central vision and colour vision. It has a diameter of about 1.5 mm. This region is a region where depression occurs at the center of the macula in the retina. In general, the depth of this region can vary from person to person by 4.0 mm and 0.8 mm, but on average it is 0.25 mm. Further, when evaluating and grading retinal diseases, it is important to know the distance between the OD and the fovea. To determine and locate OD and fovea accurately and automatically, this distance is highly important [19]. In this study, a method was developed for the diagnosis of optic nerve hypoplasia, which is associated with detecting regional anatomical structures of the retina, including the OD, the macula and the fovea, where the effects of changes associated with many eye diseases can be observed early.

Optical nerve hypoplasia (ONH) occurs when the retinal ganglion cells and axons constituting the optic nerve do not develop properly. This disease is also referred to as an optic disc that is smaller than normal, and it has been found to cause significant visual dysfunctions, particularly in children [30]. Statistics indicate that ONH is among the leading causes of visual disorders in children worldwide [33]. The prevalence of ONH increased six-fold between 1970 and 2000, reaching 1.1 per 10,000 children today. Between 1970 and 2000, ONH prevalence increased six fold, reaching the current estimate of 1.1 per 10,000 children [12]. Especially in recent years, Mousa et al. reported an increase in children experiencing health problems related to visual disorders. It was stated that approximately 12% of visual impairment cases in children in the US and Europe were caused by ONH [33]. Men and women are equally affected by ONH. Although the disease rarely occurs, it is crucial to detect it accurately to prevent blindness from occurring. Every newborn child is therefore examined and calculated to determine whether or not they have this disease [12]. As shown in Figure 2, a

Figure 1
Anatomical Structures of the Retina

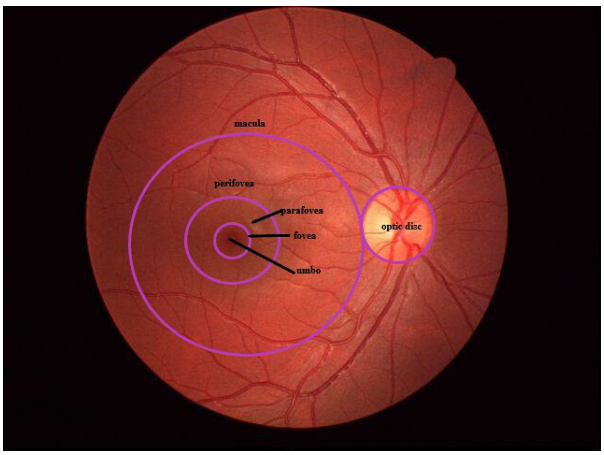

Figure 2
Parameters Used for Morphometric Techniques in the Diagnosis of ONH

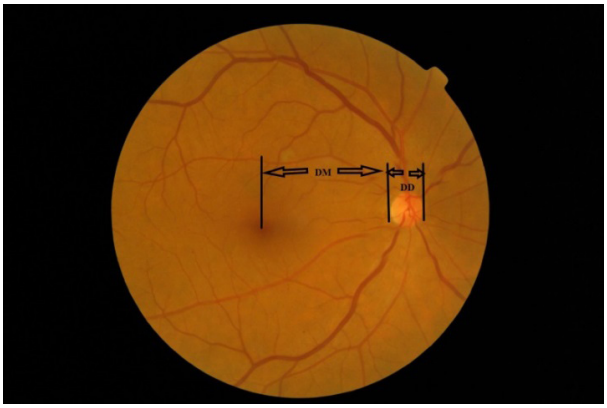

smaller ratio than 0.3 exists in ONH images between the horizontal disc diameter (DD) and the distance between the fovea center and the temporal edge of the optic disc (DM). In normal retinal images, the ratio is greater than 0.3 [30].

This study aimed to measure these parameters most accurately and quickly so that the diagnostic result had the smallest error margin possible. The diameter of the optic disc and its distance from the macula's center are manually measured in ophthalmology, and a diagnosis is based on the ratios of these measurements. Diagnosing this disease requires the use of a calculator or paper and pencil.

This study aimed to measure these parameters most accurately and quickly so that the diagnostic result had the smallest error margin possible. In ophthalmology, the diameter of the optic disc and the distance between the optic disc edge and the umbo point located at the center of the macula are manually measured, and a diagnosis is made based on the ratios of these parameters. Diagnosing this disease requires the use of a calculator or paper and pencil. This study provides doctors with a useful tool for diagnosing optic nerve hypoplasia, which had not been diagnosed before with deep learning methods. This paper makes the following major contributions:

- On retinal fundus images, boundaries of OD, OD diameter, and the umbo point, also called the macula center, were automatically detected to diagnose this disease.
- Calculations necessary for diagnosis were done automatically without the use of paper, pencil, or calculators.
- It takes a neural network less than a second to predict in an appropriate setting, while a doctor needs more time to comprehend and make a decision based on the image features. Also, deep neural networks do not get tired even if they perform the same tasks repeatedly. Thus, it helps eliminate disease risks that may have been overlooked during diagnosis.
- Combining pre-trained ResNet with U-Net provides robust performance for detecting optical nerve hypoplasia, which is a novel aspect of the proposed method.
- This method avoids overfitting by combining pre-trained ResNet and U-Net, resulting in faster network training with fewer epochs.
- We tested the proposed architecture on retinal images in Messidor, Diaretdb1, DRIVE, HRF, APTOS, and IDRID databases. Additionally, 189 retinal images obtained from Düzce University's Department of Ophthalmology were used to create a special database called ONH-NET.

2. Related Work

Automated retinal image analysis begins with OD detection.

A general classification of OD segmentation methods is shape-based, template-matching, and deformable and active contour-based. A number of segmentation methods are used in the detection of anatomical structures for the diagnosis of ONH, including gradient information-based methods, thresholding methods, shape detection methods, edge detection methods, and active contour-based methods, as in other biomedical image segmentation tasks [31]. One of the most frequently encountered problems with conventional image processing methods is that the method is valid only for a certain target dataset. As these methods have not worked in different environments and conditions, researchers are looking for a general solution with deep learning. Depending on the imaging conditions and assumptions about the acquired images, classical image segmentation techniques can be accurate [9]. Thus, automated systems based on these methods may not work for images with different properties. These issues can be solved by deep learning segmentation solutions that learn how to represent certain objects from various annotated images. Deep learning architectures can be improved to produce more reliable models through problem-specific improvement studies. This study showed the effects of such an improvement on segmenting anatomical structures like the optic disc and fovea in retinal images.

Especially in the fields of convolutional neural networks (CNNs) and medical image analysis, deep learning has shown noteworthy segmentation performances in recent years [28, 65]. Anatomical structures of the retina are increasingly being segmented with deep learning methods [26, 29]. In Table 1, CNN methods for detecting anatomical structures in retinal images are compared with existing methods. In CNN-related work, we learn how to map features in an image and use that knowledge to map them in more

Table 1
Comparison of the CNN methodologies for the detection of Retinal Anatomical Structures with the existing methods in the literature

Authors	Approach	Detected Landmarks	Databases	Success Rate
Fu et al. [9]	M-Net	Optic disc, optic cup	ORIGA, SCES	For ORIGA AUC = 0.8380 For SCES AUC = 0.8980
Wang et al. [59]	U-Net	Optic disc	DIARETDB0, DIARETDB1, DRIONSDB, DRIVE, MESSIDOR, ORGIA.	IOU=0.8910 DSC=0.9390
Gu et al.[14]	CE-Net	Optic Disc, Vessels	ORIGA, MESSİDOR, RIMONE	Sen= 0.8300, Acc=0.9500, AUC=0.9700
Wang et al. [60]	POSAL	Optic disc, optic cup	DRİSHTİ-GS, RIM-ONE, REFUGE	Diceloss of disc=0.9500 Diceloss of cup=0.8800
Al-Bander et al. [3]	CNN	The center of the Optic disc, fovea	MESSIDOR, KAGGLE	Fov cen. Acc=0.9700 OD cen Acc=0.9670
Hasan et al.[17]	DRNet	The center of Optic disc, fovea	IDRiD, RIMONE, DRISHTI-GS, DRIVE	mIoU =0.8400, mIoU =0.9000, mIoU =0.9330, mIoU =0.9200
Sevastopolsky et all.[50]	U-Net	Optic disc, optic cup	DRIONS-DB, RIM-ONE v.3, DRISHTI-GS	OD IOU= 0.8900 OC IOU=0.7500
Serener et al.[49]	GoogLeNet	Optic disc	RIM-ONE	Acc=0.8600, Se=0.2100 for R.NET Acc=0.8500, Se=02900 for G.NET
Fu et al. [10]	DENet	Optic disc	SCES, SINDI	AUC=0.9100, Acc=0.8400, Se=0.8400, Sp=0.8300 AUC=0.8100, Acc=0.7400, Se=07800, Sp=0.7100
Li, et al. [27]	RCNN	Optic disc, fovea	MESSIDOR	Jaccard = 0.8018, dice index=0.8877
Guo et al. [15]	A novel network MESNet	Optic disc, optic cup, vessel	DRIVE, STARE and CHASE	Acc=0.9667, Se=0.8200, Sp=0.9853, AUC=0.9853 Acc=0.9724, Se=0.8200, Sp=0.9897, AUC=0.9893 Acc=0.9697, Se=0.8100, Sp=0.9845, AUC=0.9869
Zhang et al. [71]	U-Net (TAU) model	Optic disc, optic cup	DRISHTIGS, RIM-ONE v3, and REFUGE	AUC=0.6200, AUC=0.7800, AUC=0.8700
Prastyo et al. [41]	U-Net	Optic disc	ORIGA	Dice coefficient score of 0. 9840, loss =0.1500

detail. Converting an image to a vector gives good results in classification problems. To segment an image, the vector created after converting a feature map into a vector must be used to reconstruct the image. Creating an image from a vector is very challenging. It is based on this problem that U-Net architecture emerged. In the same way that an image is converted to a vector, the vector is also converted back into an image using the feature mapping used during conversion. As a result, distortions in the image will be greatly reduced and the structural integrity of the image will be preserved. To detect the fovea and optic disc, this study used the U-net model, a deep learning technique commonly used in medical imaging.

3. Proposed Methodology

The purpose of this study was to develop a method to precisely segment the optic disc and fovea, which are both necessary to detect optic nerve hypoplasia. Our work is based on deep learning techniques, which have revolutionized computer vision in recent years and are providing state-of-the-art solutions for image classification, segmentation, and other tasks. Deep learning networks are trained differently from model to model, but the steps are the same. The greatest advantage of convolutional neural networks as deep learning tools is their universality since they are able to recognize many different patterns in various images and objects.

This study used U-Net-based semantic segmentation to segment the optic disc and fovea structures. The main benefit of U-net is the creation of highly detailed segmentation maps from a small number of trading samples. Having properly labelled images is very important in medical imaging, as there is a shortage of properly labelled images. It is essential to have properly labelled images in medical imaging. The network can learn these variations without additional labelled data by using random elastic deformation on the training data [2]. Separating touching objects of the same class is another challenge, which can be overcome using a weighted loss function that penalizes the model if it fails to separate them. Due to its context-based learning, U-net also trains much faster.

These two challenges are alleviated by U-Net. The following are the advantages of U-Net over other CNN models:

- Training a network requires a limited number of samples.
- Using multi-scale recognition and fusion to realize image features.
- Structures that are simple and flexible.
- Achieving high-quality pixel-level segmentation.

Aside from providing a flexible and extensible structure, the original U-Net is also effective for medical segmentation [43, 34]. By adapting to new tasks, the improved model will be able to meet a variety of needs [61,63].

In semantic segmentation processes, pixel-based classification can be done with little training data. Because the classification process is pixel-based, images to be used for education do not have to be split into fovea, disc, and background. All three classes can coexist in the training image. Semantic segmentation architectures can train on a pixel-by-pixel basis because the label image shows what class each pixel belongs to. In this study, at the training stage, the Messidor database was used. There are 1200 colour fundus images in this database taken with a The Topcon TRC NW6 monocular retinography camera can be used for non-mydriatic retinography. It has a field of view of 45°. We divided the processed dataset into three subgroups, 900 for training, 180 for internal validation, and 120 for independent testing, based on a ratio of 0.75:0.15:0.10 [58]. Segmenting retinal images requires annotating input images for segmentation training. In Ground truth for Messidor's database, fovea was not provided. The ground truth for the annotation of the optic disc and fovea was obtained from a manual label made by an ophthalmologist, the third author of this paper. LabelMe [61], a free and open-source annotation tool developed by MIT, was used for marking optic disc and fovea boundaries and binding boxes for the segmentation of ground truth. LabelMe lets you label images and create annotated masks on the web. LabelMe has been used to map retinal regions and then generate the image mask from the original image to annotate our retinal images.

As a pre-processing step, grayscale conversion and resizing processes were applied to the images before training began. U-Net is a convolutional neural network segmentation architecture that is fully connected. (https://github.com/seva100/optic-nerve-cnn).

Due to its shape, it was named after the letter U. Encoders and decoders are the two parts of this architecture [51]. In the encoder part, discriminative features are extracted from the image via convolutional layers. In the convolution layer, there are three 3*3 filters, whereas the maximum pooling layer has two 2*2 filters. Encoder part is an iterative convolution operation where the ReLU and max pooling (2x2 max pooling) operations are applied, followed by each convolution. The bottommost layer serves as a mediator between the encoder layer and the decoder layer. It consists of CNN layers followed by an upper convolution layer. Feature information is increased while spatial information is decreased, thus enabling the architecture to learn complex structures more effectively during contracting. Expansion paths, also

known as decoders, are symmetrical paths in which precise localization is achieved by transposed convolutions. Therefore, it is a completely convolutional network from end to end, that is, it does not contain any dense layers, but only consists of convolutional layers. Therefore, it can be applied to any image. CNN layers receive input from the expansion layer, which is then passed on to the upsampling layer. When the input is added (depth concatenation), the contraction layer's attribute map corresponds to the current expansion layer. This action will ensure that the attributes learned when shrinking the image are used to reconstruct it. Additionally, the convolutional layer uses half as many feature maps after each block to maintain symmetry. There is the same number of expansion blocks as contraction blocks. After passing through these blocks, the resulting mapping is passed through a 3x3 CNN layer with as many cluster feature maps as there are clusters to be reached. Therefore, while solving the segmentation problem, multiclass classification is also performed at the same time, so that each pixel is classified accordingly [46].

Our U-Net architecture is shown in Figure 3 of this study. There are four blocks in the encoder phase of a proposed U-Net model, each containing two 3x3 convolutional layers. The output of each block is connected to a max pool layer. Like the encoder phase, the decoder phase uses the same blocks, except that the max-pooling layers are replaced by upsampling layers. Batch Normalization (BN) and ReLU layers are included in both the encoder and decoder stages. Using batch normalization, a convolutional neural network can be made more regular. In other words, it normalizes the input layer by scaling the convolutional neural network, making the model more stable and faster. The ReLU function is nonlinear. For negative inputs, ReLU returns 0, while for positive inputs, x returns x. In the encoder part of the pooling layer, the weight parameters are transmitted to the next layer with the maximum pooling method. The unspooling layer can be expressed as performing this process in the decoder phase. A maximum value from each set is selected in the max-pooling layer to reduce the resolution of the image. Data size reduction was the main purpose of this layer.

The number of first feature maps was taken as 16 and model training was carried out to increase to 32, 64,128,256 throughout the layer. Lastly, the output layer calculated values between 0-1 using the sig-

Figure 3

Proposed U-Net Architecture used to find Optic Disc and Fovea

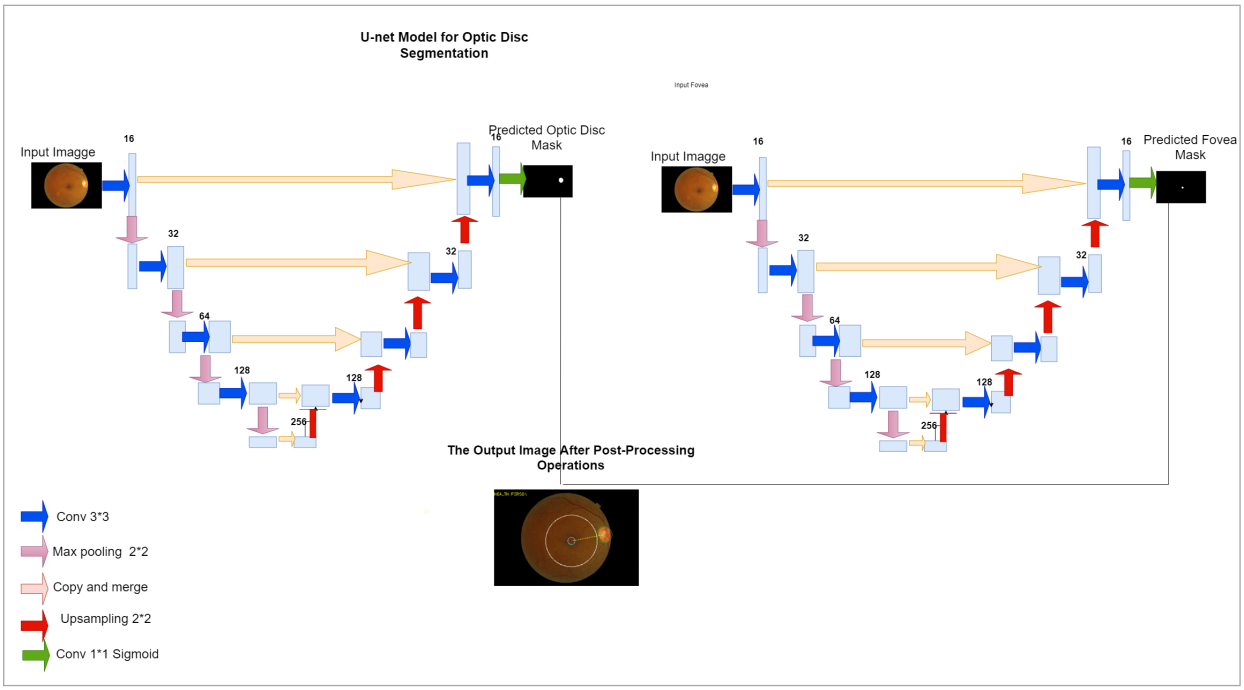

Table 2
List of hyper-parameters and their ranges/values

Hyper-parameter	Configuration
Learning rate	0.001
Number of epochs	100
Optimizer	Adam
Batch Size	64
Dropout rate	30
Filter	32,64,128,256,512
Loss Function	dice_coef_loss
Metric	Intersection over Union (IOU), Accuracy

moid function. The Adam method was used as the optimization algorithm of the model, and all other hyper-parameter settings that were used in the model are shown in Table 2. In this study, the Adam method was used due to its ease of application, efficiency in calculation, low memory requirement, invariance to diagonal rescaling, and suitability for large dataset problems [25]. This method can also be used for non-stationary objectives and noise- or sparse-gradient problems. The learning rate in Table 2 is user-defined values that typically range from 0 to 1. Training and testing the model take longer if the learning rate is too slow. The learning rate, however, may not provide an optimal value at a certain point if it is too high. We tested the learning rate at 0.1, 0.01, 0.001 and 0.0001 for this study, and the best result was 0.001.

In CNN models, millions of weights have to be learned in both the convolutional and fully connected layers. The training dataset needs to be big with a lot of images so that the weights can be optimized. It is hard to find such a dataset for problems like surface defect detection, though. Typically, this problem is solved with pre-trained network architectures or by increasing the number of samples in the dataset with data augmentation methods. The use of data augmentation is particularly useful when there are relatively few training samples. Large-scale models can be trained more robustly this way. In this way, the data augmentation process prevents problems caused by low numbers of data units and the model's memory behavior [67]. This study uses various augmentation methods to increase the number of data points, including flipping, mirroring and cropping. Although data augmentation methods add more samples to a data set, they can be insufficient, especially when there is a lot of similarity between classes. Furthermore, when small defects are small and very similar to the background, the disappearance of negative samples or blurring may not distinguish the surface error in data augmentation methods. When viewing abnormal fundus images, it can be challenging to segment the optic disc and fovea due to various distractions, such as variations in illumination, blurry boundaries, and occlusion of retinal vessels. In these situations, it will be more advantageous to use pre-trained network architecture [14]. For more accurate segmentation results, a modified U-Net architecture was developed that combines popular pre-trained ResNet-18 models with classical U-Net decoding layers as coding layers. For optic disc and fovea segmentation, ResNet pre-trained with ImageNet dataset is combined with UNet architecture. Using pre-trained ResNet weights as the decoding layers has several advantages. Firstly, a classical U-Net needs to be trained from scratch, which usually requires a longer training period. Comparatively, pre-trained weights are used in the proposed architecture, thus requiring fewer training periods.

ResNet won first place for classification, detection, and localization in an ImageNet competition [14]. By using residual convolutions, ResNet improves feature use and network performance. Furthermore, the residual mechanism maintains high performance while adding depth to the network. As networks get deeper, this mechanism has also reduced gradient loss. A residual skip-connection has been proposed as a robust alternative to the U-Net skip-connection, which concatenates encoder features and decoder features. The ResNet-18 model is adapted to U-Net by convolution of the previous layer's output by 2x2 and the encoder part by 1x1 to obtain the decoding blocks. Before going into the next decoder block, the combined tensor is batch-normalized. This final layer is also convolution-transposed with the same plane number as the target classes and with the same size as the output image.

Xiuqin and friends, proposed the ResUnet method, which combines U-Net with a residual learning strategy, to segment retinal blood vessels accurately. As a result of the proposed algorithm, the complexity of the network decreased as well as the accuracy of segmentation increased [66]. Based on retinal images, Baid and friends developed a Convolutional Neural Network (CNN)-based system that predicts Pathological Myopia. Their novel Residual UNet architecture has also been used to segment the optic disc from the retinal images [6]. As reported by Puchaicela-Lozano et al.,

the researchers proposed a hybrid approach for glaucoma fundus image localization utilizing pre-trained region-based convolutional neural networks (R-CNNs) ResNet-50 and cup-to-disk segmentation [42]. The U-Net architecture was modified in order to develop a robust segmentation method for optic disc and fovea segmentation, combining widely used pre-trained segmentation algorithms. The ResNet-34 model consists of encoding layers and classic U-Net decoding layers [68]. Compared to ground truth values, their correlation agreement is over 80% and their mean absolute error is less than 0.08. The Weighted Res-UNet was proposed by Xiao and friends to address the challenging retinal vessel segmentation problem by incorporating weighted attention and skip-connecting strategies. A baseline model is implemented with no attention and without skip connections [64]. Our method differs from studies conducted with traditional U-net in the following ways:

- With the addition of ResNet's residual learning module to the U-Net architecture, we propose Res-UNet, which increases learning ability and training efficiency. The network learns the optimal representational features through the filters, so no handcrafted features are required.
- Using the trained classifier, a segmentation map is obtained for each retinal image. A bright blob around the retinal image edge or lesions could be misinterpreted as an optic disc. Finally, post-processing is performed on the segmentation map to eliminate disturbance pixels.
- Fovea boundaries become nonsharp due to poor or overexposed illumination, including light reflections from the light source of the camera. With the proposed method, segmentation of the real fovea region is achieved.

In addition, DropOut and batch normalization were applied with 0.3 probability to prevent overfitting. Moreover, using the early stopping function during training prevented the network from memorizing, allowing the training to stop at the optimal point with this function, training stops if there are no differences in the loss function after 10 iterations. A model between actual and predicted values was analyzed using the dice_coef_loss function, which is defined in Equation 1.

$$DC(p_i, t_i) = \frac{2\sum_{i=1}^{N} p_i t_i}{\sum_{i=1}^{N} p_i + \sum_{i=1}^{N} t_i}. \quad (1)$$

The Dice coefficient, which is shown as DC in the equation represents the overlap between a probabilistic map and the ground truth that is used to determine the difference between the two. As shown in the equation, t_i represents the ground truth class, and p_i represents the probabilistic class. There is a better effect on measuring small objectives [21]. The model's accuracy and loss curves are shown in Figure 4.

Figure 4

Training and validation loss curve and accuracy curve

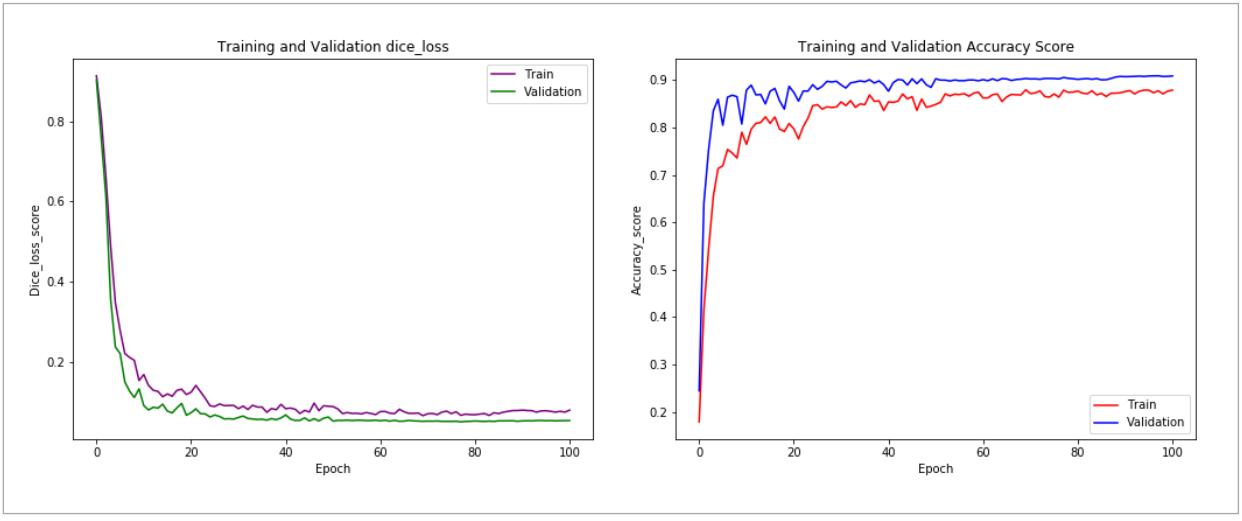

4. Experimental Results for U-Net Model

In the literature, there are several open-access databases on which disease analysis can be made from fundus images. In this study, the test stage took place on images in the Messidor, IDRID, STARE, DRIVE, DIARETDB0 and DIARETDB1, HRF, and APTOS databases shown in Table 3. In addition, a special database called ONH-NET was created based on 189 retinal images obtained from Düzce University, Department of Ophthalmology. In order to use these images in this study, an ethics committee report was obtained from Duzce University Department of Ophthalmology.

By using our method, each segmentation is quantified in terms of Sensitivity, Recall, Precision, F-score (Dice Coefficient), and IOU (Jaccard Index). Table 4 defines these performance metrics. A True Positive (TP) indicates how many pixels are correctly predicted to be OD pixels; a True Negative (TN) indicates how many pixels are correctly detected to be non-OD pixels; a False Positive (FP) indicates pixels that are incorrectly identified as OD pixels; and a False Negative (FN) indicates pixels that are incorrectly identified as non-OD pixels. All accuracy criteria listed above were calculated for the OD measurement of colour retinal images found in different databases. For evaluating the model's performance, accuracy criteria were calculated, after first training the proposed model and then testing it a few times. Using the images from MESSIDOR, IDRID, DIARETDB1, HRF, DRIVE, and APTOS databases, as well as images obtained from the Düzce University Research Hospital's Department of Ophthalmology, Table 5 shows the model's accuracy metric criteria.

In Table 6, the study's model is compared to other methods according to the metrics shown in Table 5. A review of the literature summarizes the results of OD segmentation using different methods on the same dataset in Table 6. A comparison is made based on Specificity, Recall, Precision, and F-score (Dice Coefficient), IOU (Jaccard Index). Comparing our method with previous approaches, we find that we outperform most previous approaches on most metrics and have comparable quality with other approaches.

In this study, applications about the segmentation of the fovea which is known as the center of the macula, which is difficult to detect with the naked eye, were also carried out. Figure 5 shows the segmented images of OD and fovea.

Table 3

Most frequently used databases for the detection of anatomical structures

Dataset Name	Number of mages	Resolution	Camera	Availability	Source
Messidor	1200	1440×960, 2240×1488 2304×1536	Topcon TRC NW6 with a color video 3CCD camera, non-mydriatic retinography device with FOV 45°	Available on registration	Decenciere et al. [8]
IDRID	516	4288×2848	The Kowa VX-10 alpha digital fundus camera, FOV 50°	Available online	Porwal et al. [40]
DIARETDB0	130	1500×1152	Unknown camera settings on digital fundus cameras, FOV 50°	Available online	Kauppi et al. [24]
DIARETDB1	89	1500×1152	ZEISS FF , with a 50-degree field of view fundus camera	Available online	Kauppi et al. [23]
STARE	400	700×605	FOV 35° for TRV50 fundus camera	Available online	Hoover et al. [18]
DRIVE	40	768×584	Non-mydriatic Canon CR5 3CCD camera with 45° FOV	Available online	Staal et al. [53]
HRF	45	3504×2336	The Canon CR-1 fundus camera has a 45-degree field of view	Available online	Budai et al. [7]
APTOS-2019	5590	Varying	Varying	Available online	Tsiknakis et al. [55]

Table 4
Performance Measure Formulas

Performance Measure	Formula
IOU=Jaccard Index [13]	TP/(TP+FP+FN)
Dice Coefficient=F1 Score[13]	2*Precision*Recall/(Precision+Recall) or (2*TP)/(2*TP+FP+FN)
Precision[69]	TP/(TP+FP)
Accuracy [69]	(TP+TN)/(TP+TN+FP+FN)
Sensitivity=Recall [69]	TP/(TP+FN)

Table 5
Performance metric measurements for disc and cup segmentation

	Accuracy Metrics			
	IOU	Sensitivity	Dice Coefficient	Precision
MESSIDOR	0.9069	0.9626	0.9505	0.9411
IDRID	0.8613	0.8968	0.9071	0.9612
DIARETDB1	0.8527	0.8892	0.8919	0.9608
HRF	0.8912	0.9248	0.9422	0.9629
DRIVE	0.7940	0.8510	0.8690	0.9094
APTOS	0.8937	0.9588	0.9393	0.9320
ONH-NET	0.8619	0.8816	0.9241	0.9751

Table 6
Comparative performance of optic disc boundary segmentation to previous methods

STUDİES	MESSİDOR				
	Jaccard	Dice Coefficient	Accuracy	Precision	Sensitivity
Wang et al. [58]	0.9326	0.9646	-	-	-
Morales et al. [32]	0.8228	-	0.9949	-	0.8950
Abdullah et al. 1]	-	0.9339	0.9989	-	0.8954
Al-Bander et al. [3]	-	-	0.9689	-	-
Roychowdhury et al. [47]	-	-	0.9956	-	0.9043
Wang et al. [59]	0.8940	0.9400	0.9700	-	0.9420
Araújo et al. [5]	0.8800	0.9300	-	-	-
Zou et al. [72]	0.8483	-	0.9981	-	0.9119
Our Method	**0.9069**	**0.9505**	**0.9974**	**0.9411**	**0.9626**
	IDRID				
	Jaccard	Dice Coefficient	Accuracy	Precision	Sensitivity
Hasan et al. [17]	0.8450	-	0.9970	-	0.8990
Porwal et al. [39]	0.7117	0.8023	-	-	-
Oza et al. [37]	-	-	-	0.9815	-
Siddiquee et al. [52]	-	0.9275	0.9970	-	-
Our Method	**0.8613**	**0.9071**	**0.9974**	**0.9612**	**0.8968**

	DRIVE				
	Jaccard	Dice Coefficient	Accuracy	Precision	Sensitivity
Wang et al. [59]	0.7780	0.8630	0.8950	-	0.7900
Morales et al. [32]	0.7163	-	0.9903	-	0.8169
Abdullah et al. [1]	-	0.8720	0.9672	-	0.8187
Salazar-Gonzalez et al. [48]	-	-	0.9412	-	0.7512
Welfer et al. [62]	-	-	-	0.8938	0.8354
Our Method	**0.7940**	**0.8690**	**0.9661**	**0.9094**	**0.8510**
	DIARETDB1				
	Jaccard	Dice Coefficient	Accuracy	Precision	Sensitivity
Wang et al. [59]	0.8330	0.9040	0.9340	-	0.8690
Abdullah et al. [1]	-	0.8910	0.9772	-	0.8510
Oza et al. [37]	-	-	-	0.9775	-
Harangi et al. [16]	-	-	-	0.9888	-
Our Method	**0.8527**	**0.8919**	**0.9773**	**0.9608**	**0.8892**
	HRF				
	Jaccard	Dice Coefficient	Accuracy	Precision	Sensitivity
Zahoor et al. [70]	-	0.9282	0.9774	0.9408	0.9233
Rodrigues et al. [45]	-	-	0.9472	-	0.7223
Ramani et al. [44]	-	0.8713	0.9667	-	0.8456
Our Method	**0.8912**	**0.9422**	**0.9683**	**0.9629**	**0.9248**
	APTOS				
	Jaccard	Dice Coefficient	Accuracy	Precision	Sensitivity
Karki et al. [22]	-	0.6700	0.8200	-	-
Our Method	**0.8937**	**0.9393**	**0.9781**	**0.9320**	**0.9588**

Figure 5

a - Segmentation Images of Optic Disc b- Segmentation Images of Fovea

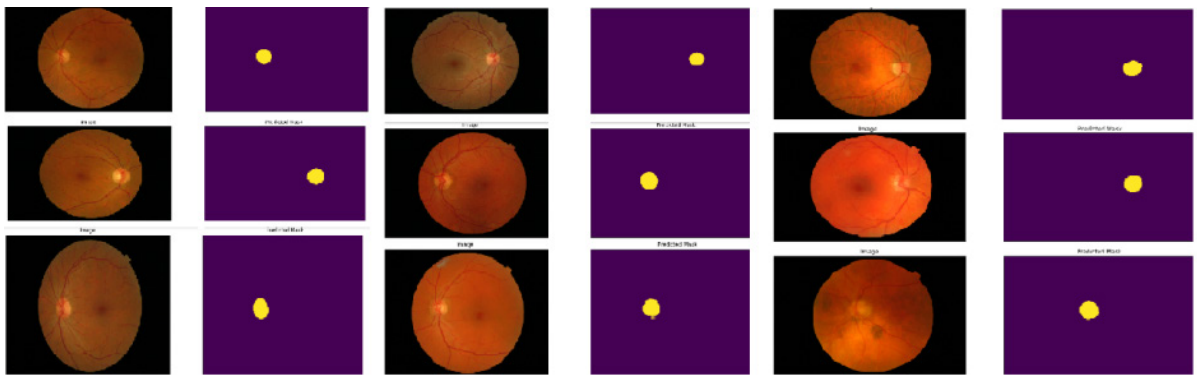

(a) (b)

5. Post-Processing for Diagnosing Optic Nerve Hypoplasia

Parameters such as the diameter of OD, boundaries of OD and the distance between OD and the center of the fovea are parameters that are required for the detection of ONH. Two separate models obtained with a U-Net-based semantic segmentation operation were loaded onto the system as shown in Figure 7. Image moments were used to determine different features of contours like the area, circumference, center and bounding box belonging to OD and the fovea. As used in image processing, computer vision, and other related fields, an image moment is a weighted average of the intensity of pixels in the image or a function of such moments. Such moments are usually selected because they have some attractive property or interpretation. f(x, y), which is a continuous 2-dimensional function has the moment of the order (p + q) is defined in equation 2 below [52].

$$M_{pg} = \int_{-\infty}^{\infty}\int_{-\infty}^{\infty} x^p y^q f(x,y)dxdy \quad (2)$$

for p,q = 0,1,2,... Adapting this to a scalar (grayscale) image with pixel intensities I(x,y), the raw image moments Mij are calculated by

$$M_{ij} = \sum_x \sum_y x^p y^j I(x,y). \quad (3)$$

In some cases, it may be possible to calculate this by considering the image as a probability density function, e.g., by dividing the above by

$$\sum_x \sum_y I(x,y) \quad (4)$$

$$\text{Area of binary images} = M_{00}. \quad (5)$$

This way, the central coordinates and radius information of OD and the fovea were obtained. After these operations, by drawing circles for which we knew the center points and radii as shown in figure 6, the boundaries of OD and the fovea were obtained. To be able to draw the macula region in the image, the distance between the central coordinates of OD and the central coordinates of the fovea is calculated using the formula $\sqrt{(OD_y - F_y)^2 + (OD_x - F_x)^2}$. In this formula, OD_y is the central y-coordinate of OD, OD_x is the central x-coordinate of OD, F_y is the central y-coordinate of the fovea, and F_x is the central x-coordinate of the fovea. From the difference between the distance found here and the diameter of OD, the radius of the macula is found.

With this operation, as shown in Figure 6, the boundaries of the macula were also obtained. Hence, all information required for the diagnosis of the disease was acquired. In light of these data, the diagnosis of the disease was decided based on the ratio of the OD diameter to the macula radius. If this ratio was smaller than 0.3, it was concluded that the image showed ONH. Therefore, the images where ONH was present were determined by looking at the diameter of OD and the distance of the fovea center to the boundary of OD.

Hence, all information required for the diagnosis of the disease was acquired. In light of these data, the diagnosis of the disease was decided based on the ratio of the OD diameter to the macula radius. If this ratio was smaller than 0.3, it was concluded that the image showed ONH. Therefore, the images where ONH was present were determined by looking at the diameter of OD and the distance of the fovea center to the boundary of OD.

Figure 6
Structures detected in ONH disease diagnosis

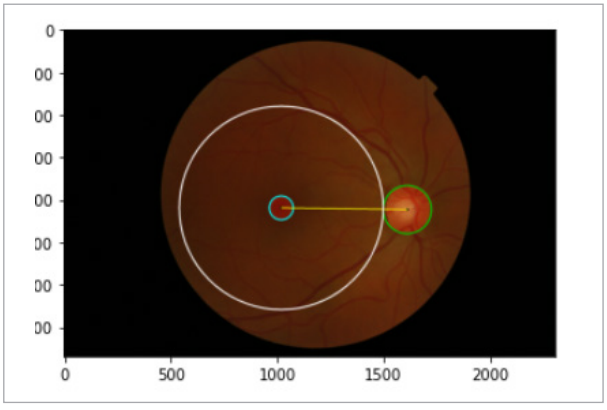

The results of applying the classical u-net model and the modified u-net model to images in the Messidor database are shown in Table 7. According to the results, the res-net architecture modified with u-net resulted in more successful results for both the foveal area and the optic disc. Figure 8 shows the images obtained with the ONH algorithm that we developed

Table 7
Results for Optic Disc and Fovea Segmentation

Method	OPTIC DISC				FOVEA			
	IOU	Sensitivity	Dice Coefficient	Precision	IOU	Sensitivity	Dice Coefficient	Precision
Modified U-net	0.9069	0.9626	0.9505	0.9411	0.8282	0.8442	0.7873	0.8252
Original U-Net	0.8613	0.8968	0.9071	0.9612	0.7268	0.76678	0.7546	0.8456

Figure 7
Flow Chart Diagram for the Diagnosis of Optic Nerve Hypoplasia

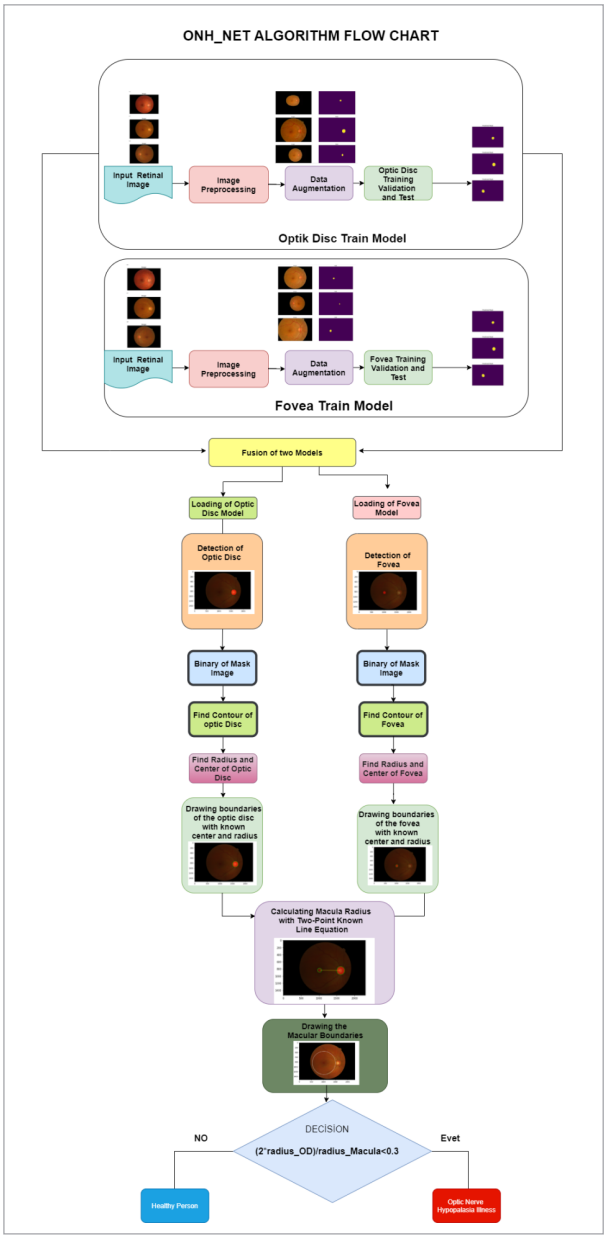

in this study. In the literature, several methods that are used for automatically extracting various features from retinal image. Most of these methods focus on detecting or segmenting only one feature. In our study, the boundary of OD, the center of OD, the boundary of the fovea, the center of the fovea and the distance between the centres of OD and the fovea were detected. Table 8 presents a summary of anatomical structures that were found in studies previously conducted on retinal images.

When the studies on this subject are examined, methods have been developed to find only the optic disc boundaries in some studies and only the foveal boundaries in some studies. In our study, the optic disc boundaries, center, radius value, foveal boundaries, central coordinate, macular radius and boundaries in the retina images were obtained.

Figure 8
Retinal structure obtained with the ONH algorithm

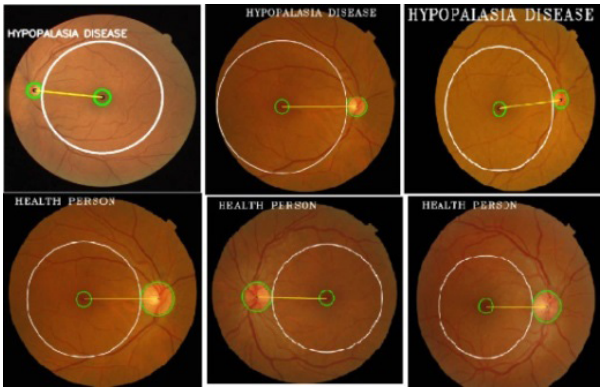

6. Conclusion

To automate diagnosis, it is highly important to find and identify retinal anatomical structures such as the optic disc, macula, and fovea at the retina, which allows early observation of changes related to many

Table 8

A comparison between the proposed methodology for optic disc (OD) and fovea (F) detection and previously used methods

Authors	Year	Approach	Detected Landmarks					Database
			Boundary of Optic Disc	Boundary of Fovea	Center of Optic Disc	Center of Fovea	Boundary of Macula	
Xie et al. [65]	2021	Fully convolutional network called SU-Net and its combination with the Viterbi algorithm	✓	X	✓	X	X	Messidor Drishti-GS
Tang et al. [54]	2021	HBA-U-Ne	✓	X	X	X	X	REFUGE , IDRID
Yu et al. [68]	2019	ResNet and U-Net	✓	X	X	X	X	RIGA, RIM-ONE Drishti-GS
Parkhi et al. [38]	2023	Deeplabv3	✓	-	✓	X	X	DRISHTI, ORIGA, and RIMONE
Wang [57]	2023	EE-UNet	✓	X	✓	X	X	REFUGE, GAMMA, Drishti-GS1, and RIM-ONE-v3, DRIONS-DB, RIM-ONE IDRID
Veena et al. [56]	2021	CNN model	✓	X	X	X	X	DRISHTI – GS
Mohan et al. [31]	2019	P-Net, which is arranged in cascade with the Fine-Net	✓	X	X	X	X	Messidor rishti-GS Drions-DB
Yamashita et al. [67]	2018	The convolutional autoencoder (CAE) network	✓	X	X	X	X	Kaggle DRISHTI GS RIM-ONE
Li et al. [27]	2018	Faster-RCNN and SVM, then RPI-based faster-RCNN	✓	✓	X	X	X	IDRID
Al-Bander et al. [15]	2018	A deep multi-scale sequential convolutional neural network (CNN)	X	X	✓	✓	X	Messidor Kaggle
Hasan et al. [17]	2021	An end-to-end encoder-decoder network, named DR-Net	✓	✓	✓	✓	X	IDRID RIMONE DRISHTI-GS DRIVE
Hussain et al. [20]	2023	UTNet	✓	X	X	X	X	DRISHTI-GS, RIM-ONE R3, and REFUGE
Tang et al. [5]	2021	HBA-U-Net	✓	✓	X	X	X	AMD, REFUGE, IDRiD
Our Method		U-Net Architecture	✓	✓	✓	✓	✓	Messidor, HRF, APTOS IDRID, DRIVE, DIARETDB1

ophthalmological diseases. The method proposed in this study not only dealt with the subject of detecting structures like the optic disc, macula and fovea but also presented a decision support system to help doctors by allowing the automated operation of procedures required for the diagnosis of the disease known as optic nerve hypoplasia that can be diagnosed with quantitative calculations. The algorithm we call ONH-NET, developed for optic nerve hypoplasia disease, which has never been diagnosed using deep learning methods before, makes the study completely original. Diagnosing optic nerve hypoplasia requires measurements such as the diameter of the optic disc, its boundaries, and the distance between the centers of the optic disc and the macula. In this study, it was aimed to measure these parameters most accurately and shortly and obtain diagnostic results with the smallest error margins. Existing techniques of optical disc and fovea segmentation have several problems, including variations in illumination, blurry boundaries, occlusion of retinal vessels, large bright lesions that obscure the fovea segmentation, and incorrect segmentation of pathological information. With the improved deep learning U-Net model, we developed a method for segmenting optic discs and fovea. An improved U-Net algorithm combined the encoding layers of the pre-trained ResNet-18 model with the decoding layers of the classical U-Net algorithm was presented in this study as a robust segmentation method for optic discs and foveas. In order to solve the problem of the traditional deep learning U-Net model requiring more depth, we added a residual module. As a result of the improved deep learning U-Net model, low-level information sharing can be prevented and performance degradation can be solved in deep convolutional neural networks under extreme depth conditions by connecting the outputs of the convolutional layer with the outputs of the deconvolution layer. Combining pre-trained ResNet with U-Net is the advantage of the proposed method. Using this method, the network is not trained from scratch, so fewer iterations are required, which prevents overfitting. After a semantic segmentation operation based on U-Net, the diameter and central coordinate information of the detected optic disc and fovea regions was reached. In line with these data, the diagnosis of the disease was decided by looking at the ratio of the optic disc diameter to the distance between the optic disc and the center of the macula. In the case that this ratio was smaller than 0.3, it was concluded that optic nerve hypoplasia was present. In the study, colour retinal images in the Messidor, Diaretdb1, DRIVE, HRF, APTOS and IDRID databases were used as the dataset. Additionally, the application was also tested on retinal images obtained from the Department of Ophthalmology at Düzce University Research Hospital. The performance values of all operations were tested using similarity indices such as the Dice and Jaccard indices, as well as sensitivity, specificity and accuracy performance criteria. An assistive tool was provided for doctors by automatically making the diagnosis of optic nerve hypoplasia, which had not been made using deep learning methods before. Hence, the calculations required for the boundaries of the optic disc, the diameter of the optic disc, the center of the fovea and the distance between the diameter of the optic disc and the radius of the macula were made in an automated manner without needing paper, pencils or calculators. Thus, ophthalmology, deep learning, and image processing skills and expertise have been successfully combined in this study for retinal image analysis and developing disease diagnosis methods. Despite the performance of the proposed method, some limitations remain. Res-UNet's probability map is sometimes discontinuous due to blood, lesions, and nerve fiber layers surrounding the OD, while some incorrect pixels may be included. It is possible to reduce the real OD region when interferences are removed by the proposed post processing. For a more reliable segmentation result, graph cut algorithms may be incorporated into post-processing, including filling OD region gaps and smoothing edges.

The retinal image analysis methods that were developed in this study were not only limited to the detection of certain anatomical structures, but they also presented a decision support system to help doctors by conducting the automated implementation of the procedures required for the diagnosis of optic nerve hypoplasia. The proposed deep learning-based approach will also be a valuable tool that could also be used for other retinal diseases.

Declarations

Conflict of interests

There are no commercial affiliations or sources of support that might pose a conflict of interest for the authors.

Authors' contributions

C. Celik and İ. Yücedağ conceived the method and conducted the system. H. T. Akçam conceived the research theme of this article, modified the paper, and guided the research. C. Celik and İ. Yücedağ conducted the verification results. All authors have made substantive contributions to the study, and all authors endorse the data and conclusions.

Financial Disclosure

The authors declared that this study had received no financial support.

Conflict of Interest

The authors certify that they have no affiliation with or financial involvement in any organization or entity with a direct financial interest in the subject matter or materials discussed in the manuscript (e.g., employment, consultancies, stock ownership, and honoraria)

Ethics

The ethics committee decision form for non-interventional health research is attached.

Availability of data and materials

In the study, colour retinal images in the Messidor, Diaretdb1, DRIVE, HRF, APTOS and IDRID databases were used as the dataset. These databases are open-access databases. Additionally, the application was also tested on retinal images obtained from the Department of Ophthalmology at Düzce University Research Hospital. Ethics committee report was obtained for retinal images taken from Düzce University, Department of Ophthalmology.

Declaration of Congress Abstract

This study has not been published or presented before.

References

1. Abdullah, M., Fraz, M. M., Barman, S. A. Localization and Segmentation and Optic Disc in Retinal Images Using Circular Hough Transform and Grow-Cut Algorithm. PeerJ, 2016, 4, e2003.https://doi.org/10.7717/peerj.2003
2. Al-Bander, B., Al-Nuaimy, W., Al-Taee, M. A., Al-Ataby, A., Zheng, Y. Automatic Feature Learning Method for Detection and Retinal Landmarks. 2016 9th International Conference on Developments in eSystems Engineering (DeSE), 2016. Liverpool. UK. 13-18. https://doi.org/10.1109/DeSE.2016.4
3. Al-Bander, B., Al-Nuaimy, W., Williams, B. M., Zheng, Y. Multiscale Sequential Convolutional Neural Networks for Simultaneous Detection and Fovea and Optic Disc. Biomedical Signal Processing and Control, 2018, 40, 91-101. https://doi.org/10.1016/j.bspc.2017.09.008
4. Almotiri, J., Elleithy, K., Elleithy, A. Retinal Vessels Segmentation Techniques and Algorithms: A Survey. Applied Sciences, 2018, 8(2), 155. https://doi.org/10.3390/app8020155
5. Araújo, T., Aresta, G., Galdran, A., Costa, P., Mendonça, A. M., Campilho, A. Uolo-Automatic Object Detection and Segmentation in Biomedical Images. Deep Learning in Medical Image Analysis and Multimodal Learning for Clinical Decision Support: 4th international Workshop, DLMIA 2018, and 8th International Workshop, ML-CDS 2018, Held in Conjunction with MICCAI 2018, Granada, Spain, September. 2018. 20-25. https://doi.org/10.1007/978-3-030-00889-5_1
6. Baid, U., Baheti, B., Dutande, P., Talbar, S. Detection and Pathological Myopia and Optic Disc Segmentation With Deep Convolutional Neural Networks. TENCON 2019-2019 IEEE Region 10 Conference (TENCON). Kochi, India, 2019, 1345-1350, https://doi.org/10.1109/TENCON.2019.8929252
7. Budai, A., Bock, R., Maier, A., Hornegger, J., Michelson, G. Robust Vessel Segmentation in Fundus Images. International Journal and Biomedical Imaging, 2013. https://doi.org/10.1155/2013/154860
8. Decencière, E., Zhang, X., Cazuguel, G., Lay, B., Cochener, B., Trone, C., Erginay, A. Feedback on a Publicly Distributed Image Database: The Messidor Database. Image analysis & Stereology, 2014, 33(3), 231-234. https://doi.org/10.5566/ias.1155
9. Fu, H., Cheng, J., Xu, Y., Wong, D. W. K., Liu, J., Cao, X. Joint Optic Disc and Cup Segmentation Based on Multi-Label Deep Network and Polar Transformation. IEEE Transactions on Medical Imaging. 2018. vol. 37, no. 7, 1597-1605. https://doi.org/10.1109/TMI.2018.2791488
10. Fu, H., Cheng, J., Xu, Y., Zhang, C., Wong, D. W. K., Liu, J., Cao, X. Disc-Aware Ensemble Network for Glaucoma Screening From Fundus Image. IEEE Transactions on Medical Imaging, 2018, 37(11), 2493-250. https://doi.org/10.1109/TMI.2018.2837012

11. Fu, Y., Chen, J., Li, J., Pan, D., Yue, X., Zhu, Y. Optic Disc Segmentation by U-Net and Probability Bubble in Abnormal Fundus Images. Pattern Recognition, 2021, 117, 107971. https://doi.org/10.1016/j.patcog.2021.107971
12. Garcia-Filion, P. An Analysis and The Prenatal History Associated With Optic Nerve Hypoplasia. (Ph.D.). University of Southern California, United States -- California. ProQuest Dissertations & Theses Global database. (3465999). 2011. Retrieved from https://www.proquest.com/dissertations-theses/analysis-prenatal-history associated-with-optic/docview/884616033/se-2?accountid=35366.
13. Ghosh, S. K., Ghosh, A. A Novel Retinal Image Segmentation Using Rsvm Boosted Convolutional Neural Network for Exudates Detection. Biomedical Signal Processing and Control, 2021, 68, 102785. https://doi.org/10.1016/j.bspc.2021.102785
14. Gu, Z., Cheng, J., Fu, H., Zhou, K., Hao, H., Zhao, Y., Liu, J. Ce-Net: Context Encoder Network for 2d Medical Image Segmentation. IEEE Transactions on Medical Imaging, 2019, 38(10), 2281-2292. https://doi.org/10.1109/TMI.2019.2903562
15. Guo, F., Li, W., Kuang, Z., Tang, J. Mes-Net: A New Network for Retinal Image Segmentation. Multimedia Tools and Applications, 2021, 80, 14767-14788. https://doi.org/10.1007/s11042-021-10580-1
16. Harangi, B., Hajdu, A. Detection and the Optic Disc in Fundus Images by Combining Probability Models. Computers in Biology and Medicine, 2015, 65, 10-24. https://doi.org/10.1016/j.compbiomed.2015.07.002
17. Hasan, M. K., Alam, M. A., Elahi, M. T. E., Roy, S., Martí, R. Drnet: Segmentation and Localization and Optic Disc and Fovea from Diabetic Retinopathy Image. Artificial intelligence in Medicine, 2021, 111, 102001. https://doi.org/10.1016/j.artmed.2020.102001
18. Hoover, A., Kouznetsova, V., Goldbaum, M. Locating Blood Vessels in Retinal Images by Piecewise Threshold Probing and a Matched Filter Response. IEEE Transactions on Medical Imaging, 2000, 19(3), 203-210. https://doi.org/10.1109/42.845178
19. Huang, Y., Zhong, Z., Yuan, J., Tang, X. Efficient and Robust Optic Disc Detection and Fovea Localization Using Region Proposal Network and Cascaded Network. Biomedical Signal Processing and Control, 2020, 60, 101939. https://doi.org/10.1016/j.bspc.2020.101939
20. Hussain, R., Basak, H. UT-Net: Combining U-Net and Transformer for Joint Optic Disc and Cup Segmentation and Glaucoma Detection. arXiv Preprint ArXiv:2303.04939, 2020. https://doi.org/10.48550/arXiv.2303.04939.
21. Jin, B., Liu, P., Wang, P., Shi, L., Zhao, J. Optic Disc Segmentation Using Attention-Based U-Net and The Improved Cross-Entropy Convolutional Neural Network. Entropy, 2020, 22(8), 844. https://doi.org/10.3390/e22080844
22. Karki, S. S., Kulkarni, P. Diabetic Retinopathy Classification Using a Combination and Efficientnets. 2021 international Conference on Emerging Smart Computing and informatics (ESCI), 2021, 68-72. https://doi.org/10.1109/ESCI50559.2021.9397035
23. Kauppi, T., Kalesnykiene, V., Kamarainen, J.-K., Lensu, L., Sorri, I., Raninen, A., Pietilä, J. The Diaretdb1 Diabetic Retinopathy Database and Evaluation Protocol. BMVC, 2007, 1(1), 10. doi: 97c88cdbe5fe375037849ef-45788dbacafddfde1.
24. Kauppi, T., Kalesnykiene, V., Kamarainen, J.-K., Lensu, L., Sorri, I., Uusitalo, H., Pietilä, J. Diaretdb0: Evaluation Database and Methodology for Diabetic Retinopathy Algorithms. Machine Vision and Pattern Recognition Research Group, Lappeenranta University of Technology, Finland, 2006, 73(1), 17. https://doi.org/bd-7d2380e76fb9dfd367d669e311d4913f67f7d2.
25. Kingma, D. P., Ba, J. Adam: A Method for Stochastic Optimization. ArXiv Preprint ArXiv:1412.6980, 2014. https://doi.org/10.48550/arXiv.1412.6980.
26. Li, T., Bo, W., Hu, C., Kang, H., Liu, H., Wang, K., Fu, H. Applications and Deep Learning in Fundus Images: A Review. Medical Image Analysis, 2021, 69, 101971. https://doi.org/10.1016/j.media.2021.101971
27. Li, X., Shen, L., Duan, J. Optic Disc and Fovea Detection Using Multi-Stage Region-Based Convolutional Neural Network. Proceedings and the 2nd international Symposium on Image Computing and Digital Medicine, 2018, 7-11. https://doi.org/10.1145/3285996.3285998
28. Litjens, G., Kooi, T., Bejnordi, B. E., Setio, A. A. A., Ciompi, F., Ghafoorian, M., Sánchez, C. I. A Survey on Deep Learning in Medical Image Analysis. Medical Image Analysis, 2017, 42, 60-88. https://doi.org/10.1016/j.media.2017.07.005
29. Maninis, K. K., Pont-Tuset, J., Arbeláez, P., Van Gool, L. Deep Retinal Image Understanding. Medical Image Computing and Computer-Assisted intervention-MICCAI 2016: 19th international Conference, Athens, Greece, October 17-21, 2016. Proceedings, Part II 19(9901). https://doi.org/10.1007/978-3-319-46723-8_17
30. McCulloch, D. L., Garcia-Fillion, P., Van Boemel, G., Borchert, M. Retinal Function in infants With Optic Nerve

Hypoplasia: Electroretinograms To Large Patterns and Photopic Flash Eye, 2007, 21(6), 712-720. https://doi.org/10.1038/sj.eye.6702309

31. Mohan, D., Kumar, J. H., Seelamantula, C. S. High-Performance Optic Disc Segmentation Using Convolutional Neural Networks. Paper presented at the 2018 25th IEEE international conference on image processing (ICIP), 2018, 4038-4042. https://doi.org/10.1109/ICIP.2018.8451543
32. Morales, S., Naranjo, V., Angulo, J., Alcañiz, M. Automatic Detection and Optic Disc Based on Pca and Mathematical Morphology. IEEE Transactions on Medical Imaging, 2013, 32(4), 786-796. https://doi.org/10.1109/TMI.2013.2238244
33. Mousa, H., Al-saboni, Y., Al-Habash, B., El Din, M. S., Al-Nashash, H. Visual Aid for Optic Nerve Hypoplasia Patients. Paper presented at the 2nd Middle East Conference on Biomedical Engineering, 2014, 127-130. https://doi.org/10.1109/MECBME.2014.6783222
34. Nawaz, M., Nazir, T., Masood, M., Ali, F., Khan, M. A., Tariq, U., Damaševičius, R. Melanoma segmentation: A Framework and Improved Densenet77 and Unet Convolutional Neural Network. International Journal of Imaging Systems and Technology, 2022, 32(6), 2137-2153. https://doi.org/10.1002/ima.22750
35. Noronha, K., Nayak, K. P. Automated Diagnosis and Diabetes Maculopathy: A Survey. Journal of Medical Imaging and Health Informatics, 2013, 3(2), 280-287. https://doi.org/10.1166/jmihi.2013.1169
36. O'Dwyer, P. A. American Academy of Ophthalmology Retina ve Vitreus, 2009. Güneş Tıp.
37. Oza, D., Nair, A., Kumar, J. H. A Novel Application and Multiscale Low-Rank Image Decomposition for Optic Disc Localization. TENCON 2019-2019 IEEE Region 10 Conference (TENCON). Kochi, India, 2019, 2690-2694. https://doi.org/10.1109/TENCON.2019.8929268
38. Parkhi, P., Hambarde, B. Optical Cup and Disc Segmentation Using Deep Learning Technique for Glaucoma Detection. International Journal of Next-Generation Computing, 2023, 14(1), 44-52. https://doi.org/d795c275-6cec-36b4-9930-ea8dfdcfc633.
39. Porwal, P., Pachade, S., Kadethankar, A., Joshi, A., Patwardhan, V., Kamble, R., Meriaudeau, F. Automatic Segmentation and Optic Disc By Gradient Minimization Based Approach. 2018 international Conference on intelligent and Advanced System (ICIAS). Kuala Lumpur, Malaysia, 2018, 1-5. https://doi.org/10.1109/ICIAS.2018.8540587
40. Porwal, P., Pachade, S., Kamble, R., Kokare, M., Deshmukh, G., Sahasrabuddhe, V., Meriaudeau, F. Indian Diabetic Retinopathy Image Dataset (Idrid): A Database for Diabetic Retinopathy Screening Research, 2018, 3(3), 25. https://doi.org/10.3390/data3030025
41. Prastyo, P. H., Sumi, A. S., Nuraini, A. Optic Cup Segmentation Using U-Net Architecture on Retinal Fundus Image. JITCE Journal of Information Technology and Computer Engineering, 2020, 4(2), 105-109. https://doi.org/10.25077/jitce.4.02.105-109.2020
42. Puchaicela-Lozano, M. S., Zhinin-Vera, L., andrade-Reyes, A. J., Baque-Arteaga, D. M., Cadena-Morejón, C., Tirado-Espín, A., Meneses, F. V. Deep Learning for Glaucoma Detection: R-CNN ResNet-50 and Image Segmentation. Journal of Advances in information Technology, 2023, 14(6). https://doi.org/10.12720/jait.14.6.1186-1197
43. Rajinikanth, V., Kadry, S., Damaševičius, R., Gnanasoundharam, J., Mohammed, M. A., Devadhas, G. G. Unet with Two-Fold Training for Effective Segmentation and Lung Section in Chest X-Ray. 22 Third international Conference on intelligent Computing Instrumentation and Control Technologies (ICICICT). Kannur, India, 2022, 977-981. https://doi.org/10.1109/ICICICT54557.2022.9917585
44. Ramani, R. G., Shanthamalar, J. J. Improved Image Processing Techniques for Optic Disc Segmentation in Retinal Fundus Images. Biomedical Signal Processing and Control, 2020, 58, 101832. https://doi.org/10.1016/j.bspc.2019.101832
45. Rodrigues, L. C., Marengoni, M. Segmentation and Optic Disc and Blood Vessels in Retinal Images Using Wavelets, Mathematical Morphology and Hessian-Based Multi-Scale Filtering. Biomedical Signal Processing and Control, 2017, 36, 39-49. https://doi.org/10.1016/j.bspc.2017.03.014
46. Ronneberger, O., Fischer, P., Brox, T. U-Net: Convolutional Networks for Biomedical Image Segmentation. Medical Image Computing and Computer-Assisted intervention - MICCAI 2015. MICCAI 2015. Lecture Notes in Computer Science, 2015, 9351, 234-241. https://doi.org/10.1007/978-3-319-24574-4_28
47. Roychowdhury, S., Koozekanani, D. D., Kuchinka, S. N., Parhi, K. K. Optic Disc Boundary and Vessel Origin Segmentation and Fundus Images. IEEE Journal and Biomedical and Health Informatics, 2015, 20(6), 1562-1574. https://doi.org/10.1109/JBHI.2015.2473159
48. Salazar-Gonzalez, A., Kaba, D., Li, Y., Liu, X. Segmentation and the Blood Vessels and Optic Disk in Retinal

Images. IEEE Journal and Biomedical and Health informatics, 2014, 18(6), 1874-1886. https://doi.org/10.1109/JBHI.2014.2302749

49. Serener, A., Serte, S. Transfer Learning for Early and Advanced Glaucoma Detection with Convolutional Neural Networks. 2019 Medical Technologies Congress (TIPTEKNO), 2019, 1-4. https://doi.org/10.1109/TIPTEKNO.2019.8894965
50. Sevastopolsky, A. Optic Disc and Cup Segmentation Methods for Glaucoma Detection with Modification and U-Net Convolutional Neural Network. Pattern Recognition and Image Analysis, 2017, 27, 618-624. https://doi.org/10.1134/S1054661817030269
51. Siddique, N., Paheding, S., Elkin, C. P., Devabhaktuni, V. U-Net and Its Variants for Medical Image Segmentation: A Review and Theory and Applications. IEEE Access, 2021, 9, 82031-82057. https://doi.org/10.1109/ACCESS.2021.3086020
52. Siddiquee, M. S., Pathan, N. S. Optic Disc Segmentation Using Superpixel Based Features and Random forest Classifier. 2019 4th International Conference on Electrical Information and Communication Technology (EICT), 2019, 1-5. https://doi.org/10.1109/EICT48899.2019.9068827
53. Staal, J., Abràmoff, M. D., Niemeijer, M., Viergever, M. A., Van Ginneken, B. Ridge-Based Vessel Segmentation in Color Images and the Retina. IEEE Transactions on Medical Imaging, 2004, 23(4), 501-509. https://doi.org/10.1109/TMI.2004.825627
54. Tang, S., Qi, Z., Granley, J., Beyeler, M. U-Net with Hierarchical Bottleneck Attention for Landmark Detection in Fundus Images and the Degenerated Retina. Ophthalmic Medical Image Analysis. OMIA 2021. Lecture Notes in Computer Science. Springer, 2021, 12970. https://doi.org/10.1007/978-3-030-87000-3_7
55. Tsiknakis, N., Theodoropoulos, D., Manikis, G., Ktistakis, E., Boutsora, O., Berto, A., Marias, K. Deep Learning for Diabetic Retinopathy Detection and Classification Based on Fundus Images: A Review. Computers in Biology and Medicine, 2021, 135, 104599. https://doi.org/10.1016/j.compbiomed.2021.104599
56. Veena, H., Muruganandham, A., Kumaran, T. S. A Novel Optic Disc and Optic Cup Segmentation Technique to Diagnose Glaucoma Using Deep Learning Convolutional Neural Network Over Retinal Fundus Images. Journal of King Saud University-Computer and Information Sciences, 2022, 34(8), 6187-6198. https://doi.org/10.1016/j.jksuci.2021.02.003
57. Wang, J., Li, X., Cheng, Y. Towards an Extended Efficientnet-Based U-Net Framework for Joint Optic Disc and Cup Segmentation in The Fundus Image. Biomedical Signal Processing and Control, 2023, 85, 104906. https://doi.org/10.1016/j.bspc.2023.104906
58. Wang, L., Gu, J., Chen, Y., Liang, Y., Zhang, W., Pu, J., Chen, H. Automated Segmentation and the Optic Disc From Fundus Images Using an Asymmetric Deep Learning Network. Pattern Recognition, 2021, 112, 107810. https://doi.org/10.1016/j.patcog.2020.107810
59. Wang, L., Liu, H., Lu, Y., Chen, H., Zhang, J., Pu, J. A Coarse-To-Fine Deep Learning Framework for Optic Disc Segmentation in Fundus Images. Biomedical Signal Processing and Control, 2019, 51, 82-89. https://doi.org/10.1016/j.bspc.2019.01.022
60. Wang, S., Yu, L., Yang, X., Fu, C.-W., Heng, P.-A. Patch-Based Output Space Adversarial Learning for Joint Optic Disc and Cup Segmentation. IEEE Transactions on Medical Imaging, 2019, 38(11), 2485-2495. https://doi.org/10.1109/TMI.2019.2899910
61. Wang, W.-T., Zhou, X.-H., Xie, X.-L., Liu, S.-Q., Huang, D.-X., Li, H., Hou, Z.-G. MEDIA-Net: Multi-scale Feature Extraction and DepthwIse Attention Network for Accurate Carotid Artery Segmentation. Procedia Computer Science, 2023, 226. 1-7. https://doi.org/10.1016/j.procs.2023.10.628
62. Welfer, D., Scharcanski, J., Marinho, D. R. A Morphologic Two-Stage Approach for Automated Optic Disk Detection in Color Eye Fundus Images. Pattern Recognition Letters, 2013, 34(5), 476-485. https://doi.org/10.1016/j.patrec.2012.12.011
63. Wu, H., Zhao, Z., Wang, Z. META-Unet: Multi-Scale Efficient Transformer Attention Unet for Fast and High-Accuracy Polyp Segmentation. IEEE Transactions on Automation Science and Engineering, 2023, 1-12. https://doi.org/10.1109/TASE.2023.3292373
64. Xiao, X., Lian, S., Luo, Z., Li, S. Weighted Res-Unet for High-Quality Retina Vessel Segmentation. 2018 9th international Conference on information Technology in Medicine and Education (ITME), 2018, 327-331. https://doi.org/10.1109/ITME.2018.00080
65. Xie, X., Niu, J., Liu, X., Chen, Z., Tang, S., Yu, S. A Survey on incorporating Domain Knowledge into Deep Learning for Medical Image Analysis. Medical Image Analysis, 2021, 69, 101985. https://doi.org/10.1016/j.media.2021.101985
66. Xiuqin, P., Zhang, Q., Zhang, H., Li, S. A Fundus Retinal Vessels Segmentation Scheme Based on The Im-

proved Deep Learning U-Net Model. IEEE Access, 2019, 7, 122634-122643. https://doi.org/10.1109/ACCESS.2019.2935138

67. Yamashita, R., Nishio, M., Do, R. K. G., Togashi, K. Convolutional Neural Networks: An Overview and Application in Radiology. Insights into Imaging, 2018, 9, 611-629. https://doi.org/10.1007/s13244-018-0639-9
68. Yu, S., Xiao, D., Frost, S., Kanagasingam, Y. Robust Optic Disc and Cup Segmentation with Deep Learning for Glaucoma Detection. Computerized Medical Imaging and Graphics, 2019, 74, 61-71. https://doi.org/10.1016/j.compmedimag.2019.02.005
69. Yu, T., Ma, Y., Li, W. Automatic Localization and Segmentation and Optic Disc in Fundus Image Using Morphology and Level Set. 2015 9th International Symposium on Medical Information and Communication Technology (ISMICT), 2015, 195-199. https://doi.org/10.1109/ISMICT.2015.7107527
70. Zahoor, M. N., Fraz, M. M. Fast Optic Disc Segmentation in Retina Using Polar Transform. IEEE Access, 2017, 5, 12293-12300. https://doi.org/10.1109/ACCESS.2017.2723320
71. Zhang, Y., Cai, X., Zhang, Y., Kang, H., Ji, X., Yuan, X. TAU: Transferable Attention U-Net for Optic Disc and Cup Segmentation. Knowledge-Based Systems, 2021, 213, 106668. https://doi.org/10.1016/j.knosys.2020.106668
72. Zou, B., Liu, Q., Yue, K., Chen, Z., Chen, J., Zhao, G. Saliency-Based Segmentation of Optic Disc in Retinal Images. Chinese Journal of Electronics, 2019, 28(1), 71-75. https://doi.org/10.1049/cje.2017.12.007